J. Fluid Mech. (2019), *vol.* 880, R2, doi:10.1017/jfm.2019.724

JFM RAPIDS
journals.cambridge.org/rapids

Transition to turbulence when the Tollmien–Schlichting and bypass routes coexist

Stefan Zammert[1,2,†] **and Bruno Eckhardt**[2,3]

[1]Laboratory for Aero and Hydrodynamics, Delft University of Technology, 2628 CD Delft, The Netherlands

[2]Fachbereich Physik, Philipps-Universität Marburg, D-35032 Marburg, Germany

[3]J.M. Burgerscentrum, Delft University of Technology, 2628 CD Delft, The Netherlands

(Received 27 February 2017; revised 22 August 2019; accepted 30 August 2019; first published online 9 October 2019)

Plane Poiseuille flow, the pressure-driven flow between parallel plates, shows a route to turbulence connected with a linear instability to Tollmien–Schlichting (TS) waves, and another route, the bypass transition, that can be triggered with finite-amplitude perturbation. We use direct numerical simulations to explore the arrangement of the different routes to turbulence among the set of initial conditions. For plates that are a distance $2H$ apart, and in a domain of width $2\pi H$ and length $2\pi H$, the subcritical instability to TS waves sets in at $Re_c = 5815$ and extends down to $Re_{TS} \approx 4884$. The bypass route becomes available above $Re_E = 459$ with the appearance of three-dimensional, finite-amplitude travelling waves. Below Re_c, TS transition appears for a tiny region of initial conditions that grows with increasing Reynolds number. Above Re_c, the previously stable region becomes unstable via TS waves, but a sharp transition to the bypass route can still be identified. Both routes lead to the same turbulent state in the final stage of the transition, but on different time scales. Similar phenomena can be expected in other flows where two or more routes to turbulence compete.

Key words: transition to turbulence, nonlinear instability, bifurcation

1. Introduction

The application of ideas from dynamical systems theory to the turbulence transition in flows without linear instability of the laminar profile, such as pipe flow or plane Couette flow, have provided a framework in which many of the observed phenomena can be rationalized. This includes the sensitive dependence on initial conditions (Darbyshire & Mullin 1995; Schmiegel & Eckhardt 1997), the appearance of exact

† Email address for correspondence: Stefan.Zammert@gmail.com

coherent states around which the turbulent state can form (Nagata 1990; Clever & Busse 1997; Waleffe 1998; Faisst & Eckhardt 2003; Wedin & Kerswell 2004; Gibson, Halcrow & Cvitanović 2009), the transience of the turbulent state (Brosa 1989; Bottin *et al.* 1998; Hof *et al.* 2006; Schneider & Eckhardt 2008; Kreilos & Eckhardt 2012), or the complex spatio-temporal dynamics in large systems (Bottin *et al.* 1998; Barkley & Tuckerman 2005; Manneville 2009; Moxey & Barkley 2010; Avila *et al.* 2011). Extensions to open external flows, such as asymptotic suction boundary layers (Kreilos *et al.* 2013; Khapko *et al.* 2013, 2014, 2016) and developing boundary layers (Cherubini *et al.* 2011*a*; Duguet *et al.* 2012; Wedin *et al.* 2014), have been proposed.

Plane Poiseuille flow (PPF), the pressure-driven flow between parallel plates, shows a transition to turbulence near a Reynolds number of approximately 1000 (Carlson, Widnall & Peeters 1982; Lemoult, Aider & Wesfreid 2012; Tuckerman *et al.* 2014). In the subcritical range the flow shows much of the transition phenomenology observed in other subcritical flows, such as plane Couette flow or pipe flow, but it also has a linear instability of the laminar profile at a Reynolds number of 5772 (Orszag 1971). This raises a question about the relation between the transition via an instability to the formation of Tollmien–Schlichting (TS) waves and the transition triggered by large-amplitude perturbations that do not need the linear instability (henceforth referred to as the 'bypass' transition) (Schmid & Henningson 2001). For instance, one could imagine that the exact coherent structures related to the bypass transition are connected to the TS waves in some kind of subcritical bifurcation. That, however, would require a connection between the two very different flow structures: the exact coherent structures that are dominated by downstream vortices (Zammert & Eckhardt 2014, 2015), and the TS waves that are dominated by spanwise vortices.

Many studies of the transition to turbulence have focused on the identification of optimal perturbations that are distinguished by being the smallest ones that can trigger the transition (Farrell 1988; Butler & Farrell 1992; Duguet, Brandt & Larsson 2010; Cherubini *et al.* 2011*b*; Monokrousos *et al.* 2011; Pringle, Willis & Kerswell 2012; Duguet *et al.* 2013). With a suitable choice of norm (for example, energy density or dissipation) this leads to an optimization problem that can be solved with suitable adjoint techniques (see Schmid (2007) and Kerswell, Pringle & Willis (2014) for reviews of the method and the connection to the dynamics in the state space of the system). In the presence of two possible routes to turbulence, via the Tollmien–Schlichting states and the bypass transition, one can expect that there are two different kinds of optimal perturbation, one for each route, but they have not been determined.

As an alternative to the determination of the optimal perturbations, we here use direct numerical simulations to map out the regions of initial conditions that follow one or the other path. Given the high dimensionality of the space, we can explore a subset of initial conditions only, and choose a plane that contains both transition states. Such explorations of the state space of a flow have been useful in the identification of the sensitive dependence on initial conditions for the transition (Schmiegel & Eckhardt 1997; Faisst & Eckhardt 2004), and in the exploration of the bifurcations (Kreilos & Eckhardt 2012; Kreilos, Eckhardt & Schneider 2014).

We start with a description of the system and the bifurcations of the relevant coherent states in § 2. Afterwards, in § 3, we describe the exploration of the state space of the system, and continue with an description of the influence of the operating conditions in § 4. Conclusions are summarized in § 5.

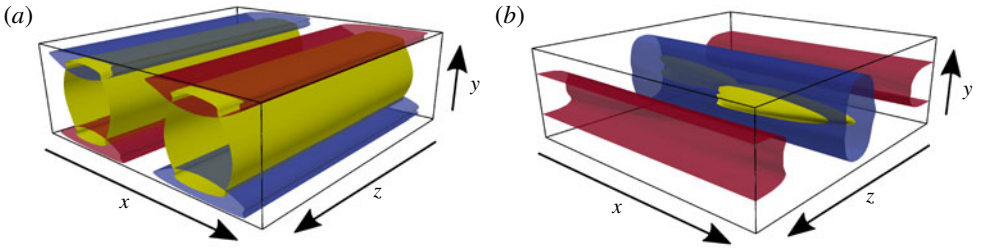

FIGURE 1. The exact coherent states for the transition to turbulence in plane Poiseuille flow. (*a*) Visualization of the Tollmien–Schlichting wave TW_{TS}. The yellow surface indicates values of $0.3Q_{max}$ for the Q-vortex criterion. The red and blue surfaces correspond to $u = \pm 0.5u_{max}$, respectively. (*b*) Visualization of the edge state TW_E for the bypass transition. As before, the yellow surface indicates values of $0.3Q_{max}$ for the Q-vortex criterion. The levels for the red and blue surfaces are now $u = 0.008$ and $u = -0.014$, respectively.

2. Plane Poiseuille flow and its coherent structures

To fix the geometry, let x, y and z be the downstream, normal and spanwise directions, and let the flow be bounded by parallel plates at $y = \pm H$. Dimensionless units are formed with the height H and the centreline velocity U_0 of the laminar parabolic profile so that the unit of time is H/U_0 and the Reynolds number becomes $Re = U_0 H/\nu$, with ν the fluid viscosity. In these units the laminar profile becomes $\boldsymbol{u}_0 = (1 - y^2)\boldsymbol{e}_x$. The equations of motion, the incompressible Navier–Stokes equations, are solved using Channelflow (Gibson 2012), with a spatial resolution of $N_x = N_z = 32$ and $N_y = 65$ for a domain of length 2π and width 2π and at fixed mass flux. The chosen resolution is sufficient to resolve the exact solutions and the transition process but under-resolved in the turbulent case. In the studied domain, the linear instability occurs at $Re_c = 5815$, slightly higher than the value found by Orszag (1971), on account of the slightly different domain size.

The full velocity field $\boldsymbol{U} = \boldsymbol{u}_0 + \boldsymbol{u}$ can be written as the sum of the laminar flow $\boldsymbol{u}_0$ and deviations $\boldsymbol{u} = (u, v, w)$. In the following we always mean $\boldsymbol{u}$ when we refer to the velocity field. To characterize the size of perturbations we will use the root mean square (r.m.s.) velocity in $\boldsymbol{u}$,

$$a(\boldsymbol{u}) = \|\boldsymbol{u}\| = \sqrt{\frac{1}{L_x L_y L_z} \int \boldsymbol{u}^2 \,\mathrm{d}x\,\mathrm{d}y\,\mathrm{d}z}, \tag{2.1}$$

or in one of the components, for example,

$$u_{rms} = \sqrt{\frac{1}{L_x L_y L_z} \int u^2 \,\mathrm{d}x\,\mathrm{d}y\,\mathrm{d}z}, \tag{2.2}$$

for the downstream component.

Tollmien–Schlichting (TS) waves are travelling waves formed by spanwise vortices. They appear in a subcritical bifurcation that extends down to $Re \approx 2610$ for a streamwise wavenumber of 1.36. The TS wave is independent of spanwise position z and consists of two spanwise vortices, as shown in figure 1(*a*).

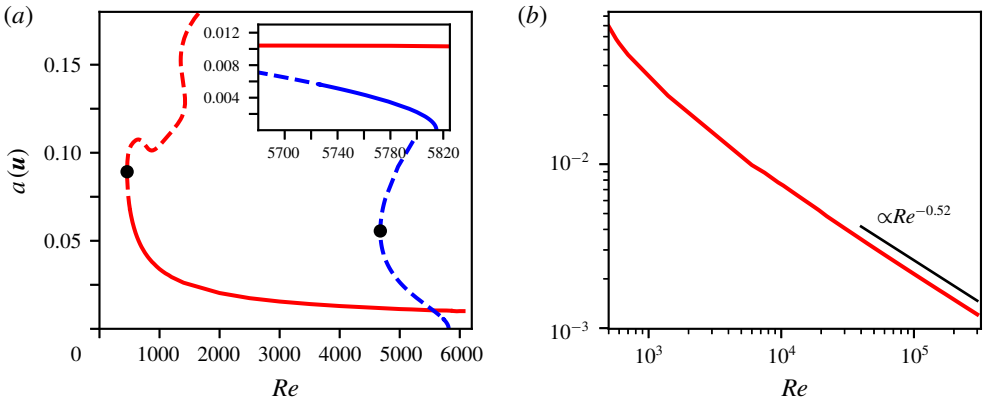

FIGURE 2. The bifurcation diagrams for TW_E (red) and TW_{TS} (blue) are shown in (a). A solid line is used if the travelling wave has just one unstable eigenvalue, while a dashed line is used when the wave has further unstable eigenvalues. The inset zooms in on the region where both waves have only one unstable eigenvalue. The bifurcation points of the waves are marked with black dots. In (b) the amplitude $a(\boldsymbol{u})$ of TW_E is shown in a double-logarithmic plot, together with a power-law decay like $Re^{-0.52}$ for large Re.

The Reynolds number range over which the transition to TS waves is subcritical depends on the domain size. For our domain (streamwise wavenumber of 1.0) the turning point is at $Re \approx 4685$. A bifurcation diagram of this exact solution, referred to as TW_{TS} in the remainder of the paper, is shown in figure 2(a). The ordinate in the bifurcation diagram is the amplitude of the deviation from laminar flow (2.1). A study of the stability of the state in the full three-dimensional space shows that this lower branch state has only one unstable direction in the used computational domain for $5727 < Re < 5815 = Re_c$. Thus, for these Reynolds numbers the state is an edge state whose stable manifold divides the state space in two parts (Skufca, Yorke & Eckhardt 2006). For lower Re, there are secondary bifurcations that add more unstable directions to the state. Specifically, near the turning point at $Re = 4690$, the lower branch has acquired approximately 350 unstable directions. Because of the high critical Reynolds numbers this state cannot explain the transition to turbulence observed in experiments at Reynolds numbers around 1000 (Carlson *et al.* 1982; Nishioka & Asai 1985; Lemoult *et al.* 2012; Lemoult, Aider & Wesfreid 2013) or even lower (Sano & Tamai 2016).

The states that are relevant to the bypass transition can be found using the method of edge tracking (Toh & Itano 2003; Schneider, Eckhardt & Yorke 2007; Schneider *et al.* 2008). Starting from an arbitrary turbulent initial condition at $Re = 1400$, trajectories in the laminar–turbulent boundary that are followed with the edge-tracking algorithm converge to a travelling wave (Zammert & Eckhardt 2014), which we referred to as TW_E in the following. After its initial identification, the state can be tracked easily to higher Reynolds numbers. The visualization in figure 1(b) shows that this state has a strong narrow upstream streak, a weaker but more extended downstream streak, and streamwise vortices. Moreover, TW_E has a wall-normal reflection symmetry

$$s_y : [u, v, w](x, y, z) = [u, -v, w](x, -y, z), \tag{2.3}$$

a shift-and-reflect symmetry

$$s_z\tau_x : [u, v, w](x, y, z) = [u, v, -w](x + 0.5 \cdot L_x, y, -z), \tag{2.4}$$

and exists for a wide range in Reynolds numbers. It is created in a saddle-node bifurcation near $Re \approx 459$ (see the bifurcation diagram in figure 2*a*); for other combinations of spanwise and streamwise wavelengths the state appears at an even lower Reynolds numbers of 319 (Zammert & Eckhardt 2017).

The corresponding lower branch state can be continued to Reynolds numbers far above 3×10^5, and its amplitude decreases with increasing Reynolds number, as shown in figure 2(*b*). A fit to the amplitude for large Reynolds numbers gives a scaling like $Re^{-0.52}$, similar to that of the solution embedded in the edge of plane Couette flow (Itano *et al.* 2013). A stability analysis of the lower branch of TW_E shows that the travelling wave has one unstable eigenvalue for $510 < Re < 5850$. Therefore, TW_E is a second travelling wave with a stable manifold that can divide the state space into two disconnected parts. How the two edge states interact and divide up the state space will be discussed in § 3.

At $Re = 510$ the lower branch undergoes a supercritical pitchfork bifurcation that breaks the s_y symmetry and adds a second unstable eigenvalue for $Re < 510$. The upper branch of the travelling wave has three unstable eigenvalues for $Re < 1000$. Investigation of different systems which show subcritical turbulence revealed that bifurcations of exact solutions connected to the edge state of the system lead to the formation of a chaotic saddle that shows transient turbulence with exponential distributed lifetimes (Kreilos & Eckhardt 2012; Ritter, Mellibovsky & Avila 2016). In the present systems the formation of chaotic saddles cannot be studied in detail since it takes place in an unstable subspace. However, previous investigations in a symmetry-restricted system did show that the states follow such a sequence of bifurcations to the formation of a chaotic saddle (Zammert & Eckhardt 2015, 2017), so that we expect that also the states in the unstable subspace follow this phenomenology.

The edge state TW_E discussed here is not identical to the travelling waves identified by Waleffe (2001) or Nagata & Deguchi (2013), as they appear at considerably higher Reynolds numbers (even for their optimal wavenumbers) and are not edge states of the system.

The two travelling waves described above are clearly related to the two different transition mechanisms that exist in the flow. For Reynolds numbers below the linear instability (here, $Re_c = 5815$), initial conditions that start close to TW_E in the state space will either decay or become turbulent without showing any approach to a TS wave: they will follow the bypass transition to turbulence. Initial conditions that start close to TW_{TS} can also either decay or swing up to turbulence, but they will first form TS waves. Above Re_c all initial conditions will show a transition to turbulence, but it will still be possible to distinguish whether they follow the bypass or TS route to turbulence, as we will see.

3. State space structure

In order to explore the arrangement of the different routes to turbulence in the space of initial conditions we pick initial conditions and integrate them until the flow either becomes turbulent or until it returns to the laminar profile. The initial conditions are taken in a two-dimensional slice of the high-dimensional space, spanned by two flow

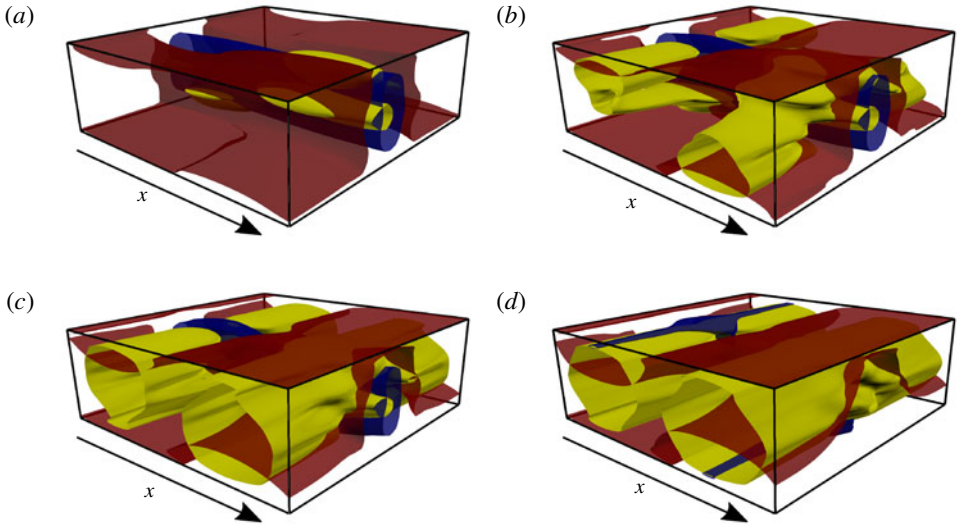

FIGURE 3. Visualizations of the velocity fields for perturbations with parameter $\alpha = 0.2$, 0.4, 0.6 and 0.8 (*a–d*, respectively) at Reynolds number 5720. The states are scaled to have an amplitude A of 0.0105. The visualizations use iso-contours of the Q-vortex criterion for $Q = 2 \times 10^{-5}$, shown in yellow. In addition, iso-surfaces for the streamwise velocity $u = 0.002$ and $u = -0.01$ are shown in red and blue, respectively.

fields $\boldsymbol{u}_1$ and $\boldsymbol{u}_2$. The choice of the flow fields allows one to explore different cross-sections of state space. For the most part, we will use $\boldsymbol{u}_1$ and $\boldsymbol{u}_2$ to be the travelling waves TW_E and TW_{TS}, so that both states are part of the cross-section. The initial conditions are then parametrized by a mixing parameter α and an amplitude A, i.e.,

$$\boldsymbol{u}(\alpha, A) = A \frac{(1-\alpha)\boldsymbol{u}_1 + \alpha \boldsymbol{u}_2}{\|(1-\alpha)\boldsymbol{u}_1 + \alpha \boldsymbol{u}_2\|}. \tag{3.1}$$

For $\alpha = 0$ one explores the state space along velocity field $\boldsymbol{u}_1$ and for $\alpha = 1$ along velocity field $\boldsymbol{u}_2$. If the upper and lower branch of TW_E are used to span such a slice, one finds that the regions in initial conditions that become turbulent have shapes that are similar to the ones in plane Couette flow (Kreilos & Eckhardt 2012; Zammert & Eckhardt 2015).

Lower branch states are on the boundary between laminar flow and turbulence, so we begin by exploring the slice spanned by the lower branches of TW_E and TW_{TS}. In figure 3, visualization for different values of α are shown. The plots illustrate how the topology of the initial flow state changes from a state dominated by streamwise streaks and vortices to a state where streaks and vortices are aligned perpendicular to the flow direction. As quantitative measures of the states, we use the r.m.s. velocity (2.2) of the individual velocity components, and the turbulent intensity

$$Tu = \sqrt{\tfrac{1}{3}(\langle u \rangle^2 + \langle v \rangle^2 + \langle w \rangle^2)}. \tag{3.2}$$

Figure 4(*a*) shows the dependence of these quantities on α. For small values of α the contribution of the streamwise component is much stronger than that of the other

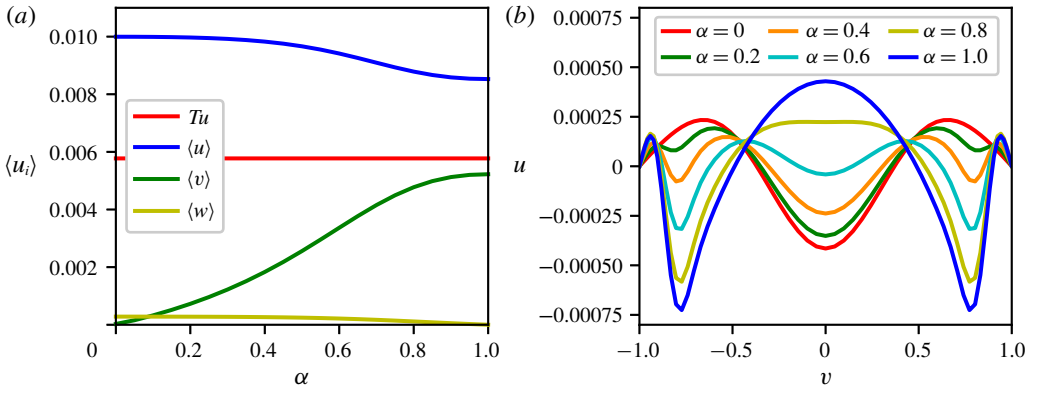

FIGURE 4. (*a*) Turbulence intensities Tu and r.m.s.-velocities $\langle u\rangle$, $\langle v\rangle$ and $\langle w\rangle$ and (*b*) mean profiles for the initial fields shown in figure 3 for different parameters α at Reynolds number 5720, and turbulence intensity Tu (red) in dependence on α. The streamwise, wall-normal and spanwise components are shown in blue, green and yellow, respectively. For $\alpha = 0$ the contribution of the wall-normal component does not vanish but is only of order 10^{-5}. (*b*) Mean streamwise velocity profiles (deviation from laminar) for different values of α.

components, due to the strong low-speed streak contained in TW_E. With increasing α the relative contribution of the wall-normal component becomes larger until for $\alpha = 1$, where we have pure spanwise rolls, it is nearly as strong as the streamwise component. In figure 4(*b*), streamwise velocity profiles for different α are shown. For low α there is a pronounced minimum in the centre of the channel, which is related to the low-speed streak of TW_E, and there are maxima close to the wall. When α is increased the profile becomes nearly inverted. For large values of α there is a maximum in the centre of the channel, and minima close to the walls.

We assign to each initial condition the time it takes to become turbulent, with an upper cutoff for initial conditions that either take longer or that never become turbulent because they return to the laminar profile. Colour-coded transition-time plots are shown in figure 5(*a–e*) for different Reynolds numbers below Re_c. The boundary between initial conditions that relaminarize and those that become turbulent stands out clearly. They are formed by the stable manifold of the states and their crossings with the cross-section. The part of the laminar–turbulent boundary connected with TW_E can be distinguished from that connected with TW_{TS} by the huge differences in transition times: for TW_{TS}, transition times are significantly longer and even exceed 2×10^4 time units. The slow growth rates of TS waves has been known for a long time. An stability analysis of the base profile shows that there is an optimal Reynolds number around $Re = 40.000$ for which the largest growth rate is obtained. But even for this Reynolds number a growth by only a factor of 10 within 300 viscous time units is achieved (Bayly, Orszag & Herbert 1988).

The interaction between the two domains is rather intricate. For Reynolds number 5780, shown in figure 5(*d*), it seems that the borders do not cross, but rather wind around each other in a spiral shape down to very small scales. Although the wave TW_{TS} has still only one unstable eigenvalue, the size of the structure that is directly connected to TW_{TS} shrinks with decreasing Re and is not visible in this kind of projection for $Re < 5727$, where TW_{TS} has more than one unstable eigenvalue. In

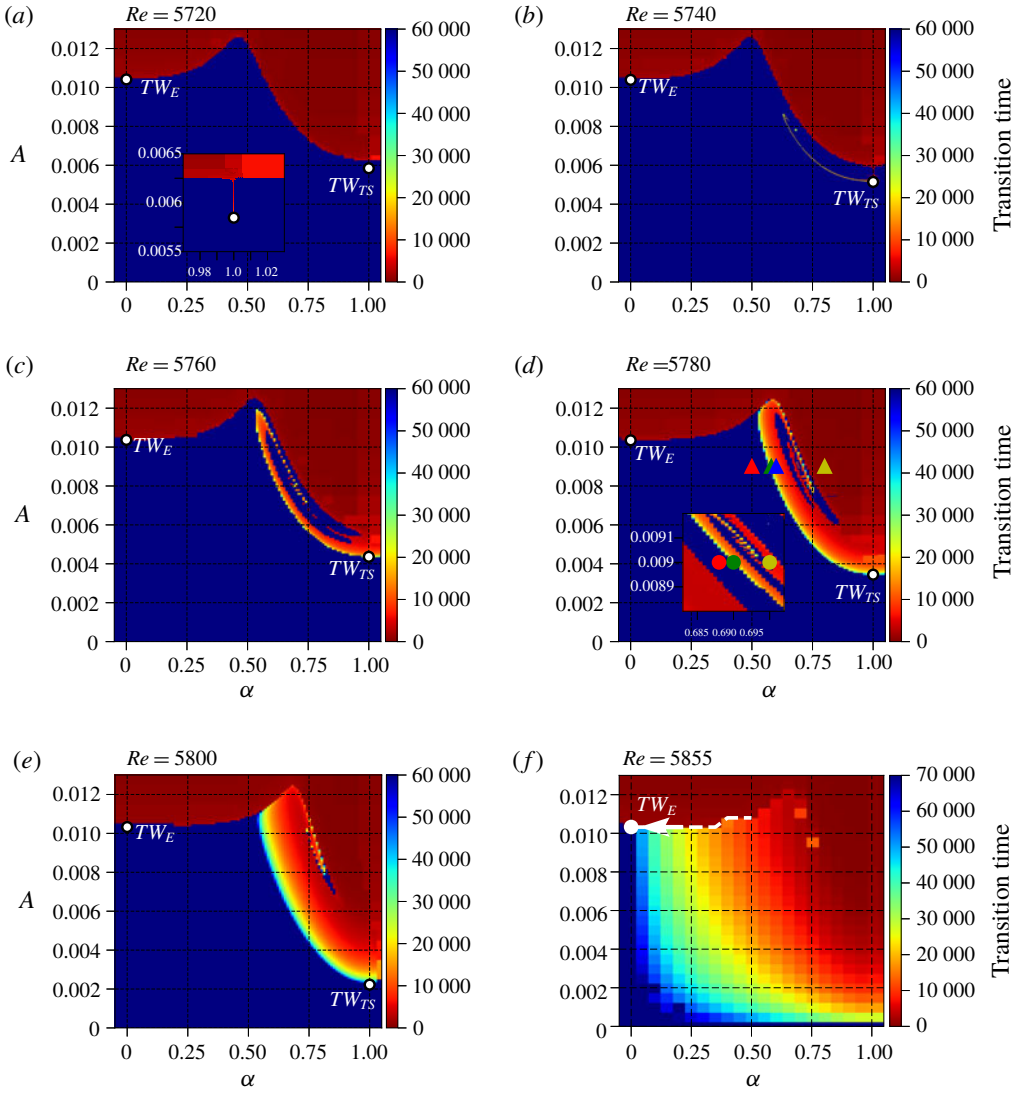

FIGURE 5. Two-dimensional slices of the state space for various Reynolds numbers. In (*a–e*), where $Re < Re_c = 5815$, the parameter α interpolates between the flow fields of both travelling waves, and both are indicated by white dots in the figures. In (*f*), where $Re > Re_c$ the plane is spanned by the flow field of TW_E and by the unstable TS mode of the laminar state. In all panels the colour indicates the time it takes to reach the turbulent states, up to a maximum integration time of 70 000 time units. Accordingly, initial conditions that do not become turbulent or return to the laminar state are indicated by dark blue. In (*f*) the dashed white line indicates the stable manifold of TW_E. The coloured triangles and dots in (*d*) mark initial conditions whose time evolution is shown in figure 6.

particular, a zoom of the area around TW_{TS} for $Re = 5720$, which is included as an inset in figure 5(*a*), shows that initial conditions which pass near TW_{TS} appear for $\alpha = 1$ only. Thus, the number of initial conditions in this projection that undergoes TS transition is of measure zero.

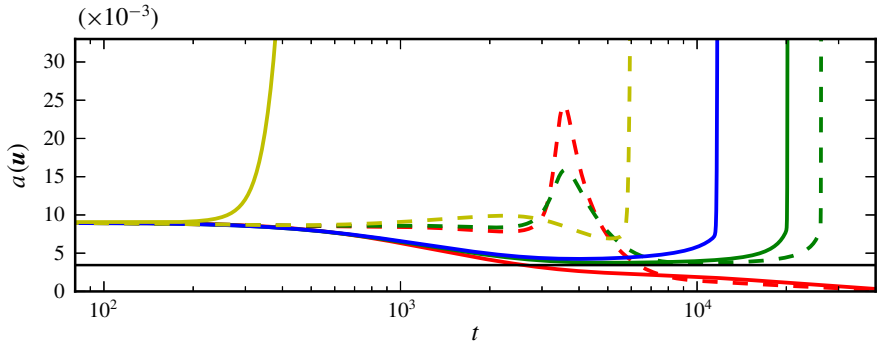

FIGURE 6. Time evolution of the velocity amplitude $a(\boldsymbol{u})$ for the initial conditions marked in figure 5(*d*) for $Re = 5780$. The initial conditions for the trajectories drawn with solid and dashed lines are marked in figure 5(*b*) with triangles and circles, respectively. The black line indicates the amplitude of the lower branch of the TS state TW_{TS} at $Re = 5780$. Some of the initial conditions that miss the bypass transition become turbulent nevertheless, because they are captured by the TS instability (for example, the full blue, and both green lines).

In figure 6 the evolution of the amplitude for different initial conditions marked in figure 5(*d*) is shown. The green and blue lines are typical representatives of the slow TS transition. Starting with a three-dimensional initial condition, their amplitude decays and the two-dimensional TS wave TW_{TS}, whose amplitude is marked by the black line, is approached.

Afterwards, they depart from TW_{TS} again, which is a slow process because of the small growth rate. As commonly known, the transition in the case of the TS transition is eventually caused by secondary instabilities of the TS waves (Herbert 1988).

The solid yellow line in figure 6 is an initial condition that undergoes bypass transition. It quickly swings up to higher amplitudes and does not approach the TS wave on its way to turbulence. The dashed yellow line is of an intermediate type. It takes a long time to become turbulent but it does not come very close to the TS wave. The relation between time evolution, transient amplification and final state is complicated and non-intuitive. For instance, the dashed red and green trajectories share a transient increase near $t \approx 4000$, but differ in their final state: the red curve, with the higher maximum, eventually returns to the laminar profile, but the green curve, with the smaller maximum, approaches the TS level and eventually becomes turbulent following the TS route. Similarly, the red, blue and green continuous lines start with high amplitude slightly below the threshold for the bypass route. They all decay, but while the red initial conditions ends up on the decaying side of the TS wave, the green and blue cases eventually become turbulent via the TS route.

For plane Couette flow it was found that a small chaotic saddle can appear inside of existing larger ones (Kreilos *et al.* 2014). There, trajectories that escape from the inner saddle are still captured by the outer saddle and thus they cannot decay directly. There is evidence that the appearance of TS transition in PPF follows a comparable but slightly different mechanism. At Reynolds number lower than 1000, the chaotic saddle related to bypass transition is created and subcritical turbulence exists. With increasing Reynolds number the chaotic saddle gets partly enclosed by the stable manifold of the TS wave, which above $Re = 5727$ can separate two parts of the state space and therefore prevent trajectories in the interior from becoming laminar.

With increasing Reynolds number the number of initial conditions becoming turbulent increases. Finally, for $Re > Re_c$, initial conditions that return to the laminar state no longer exist. Nevertheless, also in this supercritical regime a sudden change in the type of transition can be identified: when the amplitude increases and crosses the stable manifold of TW_E, the transition time drops dramatically and turbulence is reached via the bypass route. In the state space visualization for $Re = 5855$, which is shown in figure 5(f), the change of the transition type presents itself in the rapid drop of the transition time with increasing A for α values between 0 and 0.6.

In the supercritical range the stable manifold of the bypass edge state TW_E separates initial conditions undergoing the quick bypass transition from initial conditions that become turbulent by TS transition. The state space picture at a higher Reynolds number of 6000 looks qualitatively similar to the one shown in figure 5(c), including the switch from TS to bypass transition when the stable manifold of TW_E is crossed.

4. State space for constant pressure gradient

Up to this point all results were obtained by simulations which keep the bulk velocity constant. Since previous studies showed differences between the system operating at constant bulk velocity and at constant pressure gradient (Barkley 1990; Soibelman & Meron 1991), we here analyse the changes in the state space structure when forces driving the flow are changed.

If the pressure gradient is fixed the Reynolds number Re_P can be defined by using the centreline velocity of the laminar flow corresponding to the pressure gradient, together with the half-channel width and the viscosity. In dimensionless form the pressure gradient then is given by $\mathrm{d}P/\mathrm{d}x = -2/Re_P$. This definition ensures that for the laminar base flow, the pressure- and bulk-based Reynolds numbers coincide.

We chose a Reynolds number of 5780 for a comparison of two constraints. For this Reynolds number the state space structure shows the highest complexity for the case of constant bulk velocity. Using the same parametrization of initial conditions, we obtain the transition-time plot shown in figure 7. Although there are small differences from the case of constant bulk velocity – for example, the tongue-like structure connected to TW_{TS} appears to be slightly thinner – the main features are unchanged.

The relative stability to a change of the operating conditions can be rationalized by the large distance to the turning points of the solution branches. Lower branch states commonly differ only slightly between pressure and bulk Reynolds number if the distance to the turning point is large. However, these differences can become huge close to the turning point of the solution branch (e.g. Zammert 2015, chap. 3.2).

These results show that organization of the state space depends only weakly on driving with constant pressure difference or constant bulk flow, and that the slices are similar. Furthermore, since the flow states used to generate the state space slice are also solutions for the case of constant bulk velocity, but for slightly different values of the bulk Reynolds number, the calculations suggest that the obtained state space slices are to some degree robust to small disturbances of the flow fields used to generate the slices.

5. Conclusions

We have explored the coexistence of two types of transition in subcritical plane Poiseuille flow connected with the existence of states dominated by streamwise and spanwise vortices (bypass and TS transition). Probing the state space by scanning initial conditions in two-dimensional cross-sections gave information on the sets of

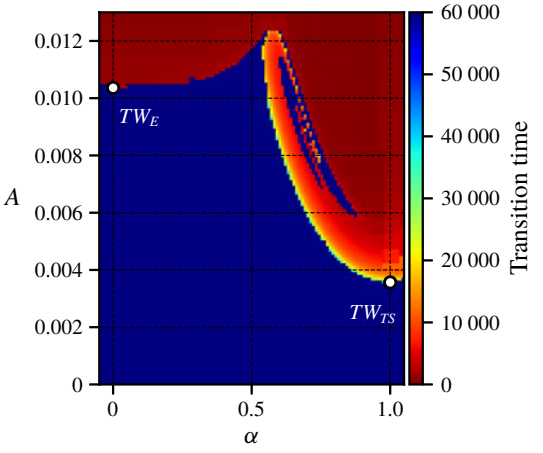

FIGURE 7. Two-dimensional slice of the state space for a pressure-based Reynolds number (Re_P) of 5780.

initial conditions that follow one or the other route to turbulence. The results show that the transition via TS waves initially occupies a tiny region of state space. As this region expands, it approaches the bypass-dominated regions, but a boundary between the two remains visible because of the very different times needed to reach turbulence. This extends to the parameter range where the laminar profile is unstable to the formation of TS waves. The investigated state TW_E lies on the border between the two transition types also for Reynolds number far above the critical one. Since its amplitude scales approximately as $Re^{-0.5}$ for high Reynolds numbers, the minimal threshold required to trigger bypass transition must decrease with this power or even faster.

The results shown here are obtained for small domains, where the extensive numerical computations for very many initial conditions are feasible. For larger domains, the corresponding exact coherent structures are localized, as shown by Jiménez (1990) and Mellibovsky & Meseguer (2015) for TS waves and by Zammert & Eckhardt (2014) for the bypass transition. Since the bifurcation diagrams for the localized states are similar to that of the extended states, we anticipate a similar phenomenology also for localized perturbations in spatially extended states.

The methods presented here can also be used to explore the relation between bypass transition and TS waves in boundary layers (Duguet *et al.* 2012; Kreilos *et al.* 2016). More generally, they can be applied to any kind of transition where two different paths compete: examples include shear-driven or convection-driven instabilities in thermal convection (Clever & Busse 1992; Zammert, Fischer & Eckhardt 2016), the interaction between transitions driven by different symmetries (Faisst & Eckhardt 2003; Wedin & Kerswell 2004; Schneider *et al.* 2008), or the interaction between the established subcritical scenario and the recently discovered linear instability in Taylor–Couette flow with a rotating outer cylinder (Deguchi 2017).

Acknowledgement

B.E. passed away on 7 August 2019 before finalization of the revision of this manuscript. He was a constant source of inspiring new ideas, an astute mind, a wonderful teacher and a good friend. He will be dearly missed.

References

AVILA, K., MOXEY, D., DE LOZAR, A., AVILA, M., BARKLEY, D. & HOF, B. 2011 The onset of turbulence in pipe flow. *Science* **333** (6039), 192–196.

BARKLEY, D. 1990 Theory and predictions for finite-amplitude waves in two-dimensional plane Poiseuille flow. *Phys. Fluids* A **2**, 955.

BARKLEY, D. & TUCKERMAN, L. 2005 Computational study of turbulent laminar patterns in Couette flow. *Phys. Rev. Lett.* **94**, 014502.

BAYLY, B., ORSZAG, S. A. & HERBERT, T. 1988 Instability mechanisms in shear-flow transition. *Annu. Rev. Fluid Mech.* **20**, 359–391.

BOTTIN, S., DAVIAUD, F., MANNEVILLE, P. & DAUCHOT, O. 1998 Discontinuous transition to spatiotemporal intermittency in plane Couette flow. *Europhys. Lett.* **43** (2), 171–176.

BROSA, U. 1989 Turbulence without strange attractor. *J. Stat. Phys.* **55** (5), 1303–1312.

BUTLER, K. M. & FARRELL, B. 1992 Three-dimensional optimal perturbations in viscous shear flow. *Phys. Fluids* A **4** (8), 1637–1650.

CARLSON, D. R., WIDNALL, S. E. & PEETERS, M. F. 1982 A flow-visualization study of transition in plane Poiseuille flow. *J. Fluid Mech.* **121**, 487–505.

CHERUBINI, S., DE PALMA, P., ROBINET, J.-C. & BOTTARO, A. 2011*a* Edge states in a boundary layer. *Phys. Fluids* **23** (5), 051705.

CHERUBINI, S., DE PALMA, P., ROBINET, J.-C. & BOTTARO, A. 2011*b* The minimal seed of turbulent transition in the boundary layer. *J. Fluid Mech.* **689**, 221–253.

CLEVER, R. M. & BUSSE, F. H. 1992 Three-dimensional convection in a horizontal fluid layer subjected to a constant shear. *J. Fluid Mech.* **234**, 511–527.

CLEVER, R. M. & BUSSE, F. H. 1997 Tertiary and quaternary solutions for plane Couette flow. *J. Fluid Mech.* **344**, 137–153.

DARBYSHIRE, A. G. & MULLIN, T. 1995 Transition to turbulence in constant-mass-flux pipe flow. *J. Fluid Mech.* **289**, 83–114.

DEGUCHI, K. 2017 Linear instability in Rayleigh-stable Taylor–Couette flow. *Phys. Rev.* E **95** (2), 021102(R).

DUGUET, Y., BRANDT, L. & LARSSON, B. R. J. 2010 Towards minimal perturbations in transitional plane Couette flow. *Phys. Rev.* E **82** (2), 026316.

DUGUET, Y., MONOKROUSOS, A., BRANDT, L. & HENNINGSON, D. S. 2013 Minimal transition thresholds in plane Couette flow. *Phys. Fluids* A **25** (8), 084103.

DUGUET, Y., SCHLATTER, P., HENNINGSON, D. S. & ECKHARDT, B. 2012 Self-sustained localized structures in a boundary-layer flow. *Phys. Rev. Lett.* **108**, 044501.

FAISST, H. & ECKHARDT, B. 2003 Traveling waves in pipe flow. *Phys. Rev. Lett.* **91**, 224502.

FAISST, H. & ECKHARDT, B. 2004 Sensitive dependence on initial conditions in transition to turbulence in pipe flow. *J. Fluid Mech.* **504**, 343–352.

FARRELL, B. F. 1988 Optimal excitation of perturbations in viscous shear flow. *Phys. Fluids* **31**, 2093–2102.

GIBSON, J. F. 2012 Channelflow: a spectral Navier–Stokes simulator in C++. *Tech. Rep.* U. New Hampshire.

GIBSON, J. F., HALCROW, J. & CVITANOVIĆ, P. 2009 Equilibrium and travelling-wave solutions of plane Couette flow. *J. Fluid Mech.* **638**, 243–266.

HERBERT, T. 1988 Secondary instability of boundary layers. *Annu. Rev. Fluid Mech.* **20**, 487–526.

HOF, B., WESTERWEEL, J., SCHNEIDER, T. M. & ECKHARDT, B. 2006 Finite lifetime of turbulence in shear flows. *Nature* **443** (7107), 59–62.

ITANO, T., AKINAGA, T., GENERALIS, S. C. & SUGIHARA-SEKI, M. 2013 Transition of planar Couette flow at infinite Reynolds numbers. *Phys. Rev. Lett.* **111**, 184502.

JIMÉNEZ, J. 1990 Transition to turbulence in two-dimensional Poiseuille flow. *J. Fluid Mech.* **218**, 265–297.

KERSWELL, R. R., PRINGLE, C. C. T. & WILLIS, A. P. 2014 An optimisation approach for analysing nonlinear stability with transition to turbulence in fluids as an exemplar. *Rep. Prog. Phys.* **77**, 085901.

KHAPKO, T., DUGUET, Y., KREILOS, T., SCHLATTER, P., ECKHARDT, B. & HENNINGSON, D. S. 2014 Complexity of localised coherent structures in a boundary-layer flow. *Eur. Phys. J.* E **37** (32), 1–12.

KHAPKO, T., KREILOS, T., SCHLATTER, P., DUGUET, Y., ECKHARDT, B. & HENNINGSON, D. S. 2013 Localized edge states in the asymptotic suction boundary layer. *J. Fluid Mech.* **717**, R6.

KHAPKO, T., KREILOS, T., SCHLATTER, P., DUGUET, Y., ECKHARDT, B. & HENNINGSON, D. S. 2016 Edge states as mediators of bypass transition in boundary-layer flows. *J. Fluid Mech.* **801**, R2.

KREILOS, T. & ECKHARDT, B. 2012 Periodic orbits near onset of chaos in plane Couette flow. *Chaos* **22** (4), 047505.

KREILOS, T., ECKHARDT, B. & SCHNEIDER, T. M. 2014 Increasing lifetimes and the growing saddles of shear flow turbulence. *Phys. Rev. Lett.* **112**, 044503.

KREILOS, T., KHAPKO, T., SCHLATTER, P., DUGUET, Y. N, HENNINGSON, D. S. & ECKHARDT, B. 2016 Bypass transition and spot nucleation in boundary layers. *Phys. Rev. Fluids* **1**, 043602.

KREILOS, T., VEBLE, G., SCHNEIDER, T. M. & ECKHARDT, B. 2013 Edge states for the turbulence transition in the asymptotic suction boundary layer. *J. Fluid Mech.* **726**, 100–122.

LEMOULT, G., AIDER, J.-L. & WESFREID, J. E. 2012 Experimental scaling law for the subcritical transition to turbulence in plane Poiseuille flow. *Phys. Rev.* E **85** (2), 025303(R).

LEMOULT, G., AIDER, J.-L. & WESFREID, J. E. 2013 Turbulent spots in a channel: large-scale flow and self-sustainability. *J. Fluid Mech.* **731**, R1.

MANNEVILLE, P. 2009 Spatiotemporal perspective on the decay of turbulence in wall-bounded flows. *Phys. Rev.* E **79**, 025301.

MELLIBOVSKY, F. & MESEGUER, A. 2015 A mechanism for streamwise localisation of nonlinear waves in shear flows. *J. Fluid Mech.* **779**, R1.

MONOKROUSOS, A., BOTTARO, A., BRANDT, L., DI VITA, A. & HENNINGSON, D. S. 2011 Nonequilibrium thermodynamics and the optimal path to turbulence in shear flows. *Phys. Rev. Lett.* **106** (13), 134502.

MOXEY, D. & BARKLEY, D. 2010 Distinct large-scale turbulent-laminar states in transitional pipe flow. *Proc. Natl Acad. Sci. USA* **107** (18), 8091–8096.

NAGATA, M. 1990 Three-dimensional finite-amplitude solutions in plane Couette flow: bifurcation from infinity. *J. Fluid Mech.* **217**, 519–527.

NAGATA, M. & DEGUCHI, K. 2013 Mirror-symmetric exact coherent states in plane Poiseuille flow. *J. Fluid Mech.* **735**, R4.

NISHIOKA, M. & ASAI, M. 1985 Some observations of the subcritical transition in plane Poiseuille flow. *J. Fluid Mech.* **150**, 441–450.

ORSZAG, S. A. 1971 Accurate solution of the Orr–Sommerfeld stability equation. *J. Fluid Mech.* **50**, 689–703.

PRINGLE, C., WILLIS, A. P. & KERSWELL, R. R. 2012 Minimal seeds for shear flow turbulence: using nonlinear transient growth to touch the edge of chaos. *J. Fluid Mech.* **702**, 415–443.

RITTER, P., MELLIBOVSKY, F. & AVILA, M. 2016 Emergence of spatio-temporal dynamics from exact coherent solutions in pipe flow. *New J. Phys.* **18**, 083031.

SANO, M. & TAMAI, K. 2016 A universal transition to turbulence in channel flow. *Nat. Phys.* **12**, 249–253.

SCHMID, P. & HENNINGSON, D. S. 2001 *Stability and Transition in Shear Flow*. Springer.

SCHMID, P. J. 2007 Nonmodal stability theory. *Annu. Rev. Fluid Mech.* **39** (1), 129–162.

SCHMIEGEL, A. & ECKHARDT, B. 1997 Fractal stability border in plane Couette flow. *Phys. Rev. Lett.* **79**, 5250.

SCHNEIDER, T. M. & ECKHARDT, B. 2008 Lifetime statistics in transitional pipe flow. *Phys. Rev.* E **78**, 046310.

SCHNEIDER, T. M., ECKHARDT, B. & YORKE, J. 2007 Turbulence transition and the edge of chaos in pipe flow. *Phys. Rev. Lett.* **99**, 034502.

SCHNEIDER, T. M., GIBSON, J. F., LAGHA, M., DE LILLO, F. & ECKHARDT, B. 2008 Laminar-turbulent boundary in plane Couette flow. *Phys. Rev.* E **78**, 037301.

SKUFCA, J., YORKE, J. A. & ECKHARDT, B. 2006 Edge of chaos in a parallel shear flow. *Phys. Rev. Lett.* **96**, 174101.

SOIBELMAN, I. & MEIRON, D. I. 1991 Finite-amplitude bifurcations in plane Poiseuille flow: two-dimensional Hopf bifurcation. *J. Fluid Mech.* **229**, 389–416.

TOH, S. & ITANO, T. 2003 A periodic-like solution in channel flow. *J. Fluid Mech.* **481**, 67–76.

TUCKERMAN, L. S., KREILOS, T., SCHROBSDORFF, H., SCHNEIDER, T. M. & GIBSON, J. F. 2014 Turbulent-laminar patterns in plane Poiseuille flow. *Phys. Fluids* **26**, 114103.

WALEFFE, F. 2001 Exact coherent structures in channel flow. *J. Fluid Mech.* **435**, 93–102.

WALEFFE, F. 1998 Three-dimensional coherent states in plane shear flows. *Phys. Rev. Lett.* **81** (19), 4140.

WEDIN, H., BOTTARO, A., HANIFI, A. & ZAMPOGNA, G. 2014 Unstable flow structures in the Blasius boundary layer. *Eur. Phys. J.* E **37** (34), 1–20.

WEDIN, H. & KERSWELL, R. R. 2004 Exact coherent structures in pipe flow: travelling wave solutions. *J. Fluid Mech.* **508**, 333–371.

ZAMMERT, S. & ECKHARDT, B. 2014 Streamwise and doubly-localised periodic orbits in plane Poiseuille flow. *J. Fluid Mech.* **761**, 348–359.

ZAMMERT, S. & ECKHARDT, B. 2015 Crisis bifurcations in plane Poiseuille flow. *Phys. Rev.* E **91**, 041003(R).

ZAMMERT, S. & ECKHARDT, B. 2017 Harbingers and latecomers – the order of appearance of exact coherent structures in plane Poiseuille flow. *J. Turbul.* **18** (2), 103–114.

ZAMMERT, S. & ECKHARDT, B. 2015 Bypass transition and subcritical turbulence in plane Poiseuille flow. *Proceedings of TSFP-9* (in press) arXiv:1506.04370.

ZAMMERT, S., FISCHER, N. & ECKHARDT, B. 2016 Transition in the asymptotic suction boundary layer over a heated plate. *J. Fluid Mech.* **803**, 175–199.

ZAMMERT, S. 2015 Localized states in the transition to turbulence in plane Poiseuille flow and thermal boundary layers. PhD thesis, Philipps-Universität Marburg.